2024 IEEE International Conference on Robotics and Automation (ICRA 2024)
May 13-17, 2024. Yokohama, Japan

Modular Growing Mechanism with Multi-axis Deformation

Dongdong Du, *Member, IEEE,* Emanuela Del Dottore, Alessio Mondini, Edoardo Sinibaldi, *Member, IEEE,* and Barbara Mazzolai, *Member, IEEE*

***Abstract*— Plant cells expand and elongate. Their cumulative actuation defines organ morphing. Inspired by this modular transformability, this study proposes a modular concept for growing robots that will be able to grow by adding at their tip Transformable Modules (TMs). We provide a two-module implementation to evaluate the concept viability. We designed and characterized Shape-Retention Bellows (SRBs) that constitute the TM and are used to maintain the shape once the extension force is relaxed. We demonstrate module radial expansion and axial elongation in a straight and bent configuration (up to ~4°). This is the first concept of growing robots to enact the robot's modularity and transformability for future deployment in distributed growing systems capable of acting in various scenarios.**

***Index Terms*— Growing robots, Shape-retention bellows, Transformable modules, Radial expansion, Axial elongation.**

I. Introduction

Biological systems are since long adopted as models in robotics to develop biomimetic systems and improve robot performance [1]. Besides animals, plants peculiar responses to environmental cues attract attention nowadays, inspiring robots [2], [3], sensors [4], [5], actuators [6], [7], grippers [8], [9], materials [10], [11], etc., broadening the research scope in robotics.

Growth is a fundamental life activity used in plants to move and navigate the environment [12]. Plant growth is localized at their apical regions [13]. This inspired a new class of robots capable of self-building their bodies, named growing robots, finding applications in environmental monitoring and exploration [14]. Sadeghi *et al.* [15] proposed the first growing mechanism using an additive layering technique: autonomously winding a thread adjacent to the tip through a rotating head. By embodying Fused Deposition Modeling 3D printing, in [16], the concept evolved into a self-growing robot that moves by apical growth and bends by differentially depositing the thermoplastic material while adapting its shape to physical constraints offered by the environment [17]. Hausladen *et al.* [18] proposed a material synthetic growing mechanism called E-SLIP that builds solid structures by photopolymerizing a monomer solution, generating pressure for material transport and pushing the head forward. Hawkes *et al.* [19] proposed a growing mechanism based on the pressurization of everting thin-walled vessels with strain-limiting fibers for programmed deployment. While impressive, the proposed mechanisms enabling apical growth do not favor a local and distributed morphing critical to enrich the behavioral domain of hyper-redundant growing robots and consequently their applicability [20]. A close look at plants shows that individual cells are the basic bricks [21]. Each cell divides, radially expands, and axially elongates [12]. While current growing robots mimic cell division merged with axial elongation through apical addition or eversion of material, there is no current solution to add radial expansion. Importantly, in plants, aggregated local deformations of individual cells shape the organ body as the expression of body-environment interaction, allowing plants to grow and navigate in space with high agility and adaptability. The cumulative effect of cell transformation might also produce additional benefits. For example, distributed cell radial expansion in roots is hypothesized to facilitate soil penetration [22], whereas, in shoots of twining plants or tendrils, it reinforces grasping force [23]. Enclosing the possibility of local and distributed deformation could enhance the morphing capability of artificial systems, improving their adaptation and resilience in challenging, mutable conditions, e.g., enabling recoveries from faults or damages [24], or provide new engineering solutions to self-construction mechanisms. However, developing modular and transformable units with multi-axis deformation while being functional to a growing mechanism is still an open challenge. While the comprehensive design of a fully operating, growing, modular robot lies beyond the scope of this work, we have taken the first step to explore the viability of the idea. This study introduces and characterizes Transformable Modules (TMs) that provide the core functionalities of axial elongation and expansion based on Shape-Retention Bellows (SRBs). Additionally, we have developed a hydraulic actuation system to validate the module transformation. We demonstrated expansion and elongation and evaluated the bending performances of the preliminary mechanism.

II. Materials and Methods

A. Robot Concept Overview

The envisioned growing robot comprises a tip and multiple ring-like Transformable Modules (TMs) (Fig. 1).

*This project has received funding from the European Research Council (ERC) under the European Union's Horizon 2020 research and innovation program (grant agreement No 101003304 – I-Wood).

Dongdong Du is with the Bioinspired Soft Robotics, Istituto Italiano di Tecnologia, 16163 Genoa, Italy, and with the College of Biosystems Engineering and Food Science, Zhejiang University, 310058 Hangzhou, PR China. (e-mail: Dongdong.du@zju.edu.cn)

Emanuela Del Dottore, Alessio Mondini, Edoardo Sinibaldi, and Barbara Mazzolai are with the Bioinspired Soft Robotics, Istituto Italiano di Tecnologia, 16163 Genoa, Italy. (e-mail: Emanuela.DelDottore@iit.it, Alessio.Mondini@iit.it, Edoardo.Sinibaldi@iit.it, barbara.mazzolai@iit.it)

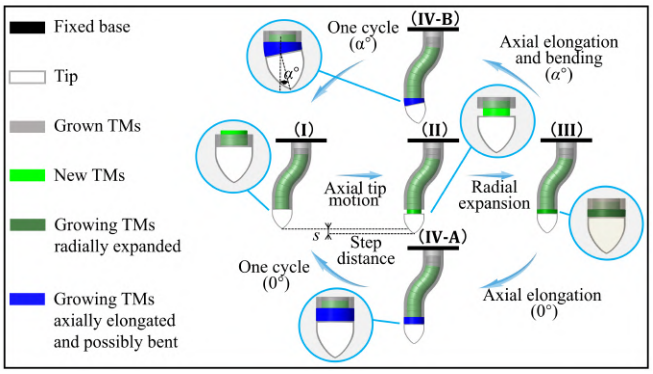

Fig. 1. Concept of the modular growing robot with its actuation flow and zoom-in on apical parts: (I) initial condition, (II) step of axial growth (the module inside emerges and pushes the tip forward), (III) module radial expansion. Then, it can (IV-A) equally axially elongate or (IV-B) differentially elongate to bend. Finally, the loop restarts.

The tip is driven by an embedded hydraulic actuation system for axial propulsion and radial enlargement. The actuation system should drive all the tip and TMs motions at different stages (new, growing, and grown). When the tip axially moves, the hydraulic actuation system is fixed to the grown body, providing the forward power. Then, new TMs run inside the grown body up to the tip, where they are radially expanded and axially elongated by the hydraulic actuation system. The new TM at the tip stably engages with the already grown TM with mechanical connections upon radial expansion, thus enacting growth. The robot continuously grows by cycling axial tip motion, TM radial expansion, axial elongation, and possibly bending. In this concept, the TMs and the hydraulic actuation system are pivotal units in implementing apical actuation. Herein, we focused on a few basic functionalities (apical displacement and its configuration) and implemented two TMs to prove the basic working principle. The tip design and the actuation system are not addressed in this paper. Whereas we provide a simplified actuation mechanism to demonstrate module transformation.

B. Design of Shape-Retention Bellow and Transformable Module

We designed Shape-Retention Bellows (SRBs) with several convolutions for multistable shape variation. The convolutions, initially compacted, elongate when applying tensile forces, and the shape is retained after force removal. This is critical for structure consolidation upon growth. This design consents to configure the module in multiple shapes (variable elongation, radial expansion and bending) and maintain the configuration stably. The multistable SRBs resemble a bellow structure, whose thickness is thinner at the neck and bottom sections and thicker at the intermediate section along the curves of each convolution (Fig. 2a). This favors the deformation at the former regions and the occurrence of two mechanically stable states (corresponding to convolutions compacted and elongated) for each convolution upon choosing a

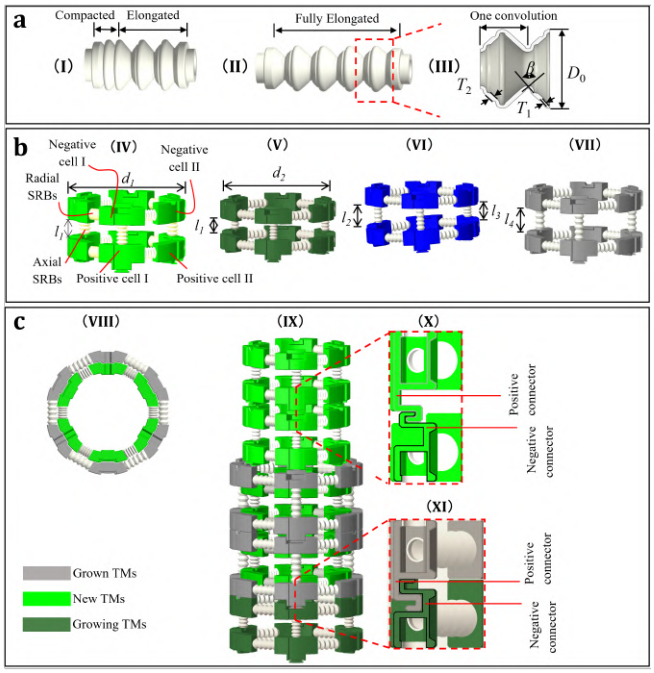

Fig. 2. SRBs and TMs design. (a) Possible configurations for the multistable SRBs. (I) Example of the SRB with two compacted convolutions; (II) SRBs with opened convolutions; (III) SRBs section and convolution parameters: diameter (D_0), thin wall thickness (T_1), thick wall thickness (T_2), and convolution angle (β). (b) TM configurations and states. (IV) A new TM its components. New TMs have a small diameter d_1 and the axial SRBs when fully compacted have length l_1; (V) a radially expanded TM has diameter $d_2 > d_1$ and compacted axial SRBs; (VI) TM axially elongated and bent (opposite SRBs have a different length, $l_2 > l_3$); (VII) TM axially elongated only (axial SRBs have a length $l_4 > l_1$). (c) Connections between TMs. (VIII) Top view of the connection between new and grown TMs; (IX) overview of the connections between TMs, with the new TMs staying inside the grown TMs; (X) section of the connection between new TMs by the double-sided connector; (XI) section of the connection between growing and grown TMs by the double-sided connector.

suitable material [25]. Multiple convolutions in a series contribute to the multistable shape variation of an SRB: the higher their number, the higher the shape variation. As for this design, thin wall thickness T_1, thick wall thickness T_2, diameter D_0, and convolution angle β are parameters influencing the SBR elongation properties.

The TMs are composed of cells and SRBs (Fig. 2b). The cells are partial ring structures distinguished in cell I to lock and cell II to align. Each type is produced in a couple with one positive and one negative cell. Three positive (negative) cells I and three positive (negative) cells II, together with six radial SRBs (arranged in a circle) responsible for radial expansion, constitute a positive (negative) half TM. The positive and negative halves are integrated into a complete TM using three axial SRBs responsible for axial elongation. Thanks to the parallel distribution of axial SRBs, different bending angles can be achieved for TMs.

We introduced a double-sided connector on cell I to connect adjacent TMs. Each connector is composed of a pair of positive and negative connectors: one side (Fig. 2c

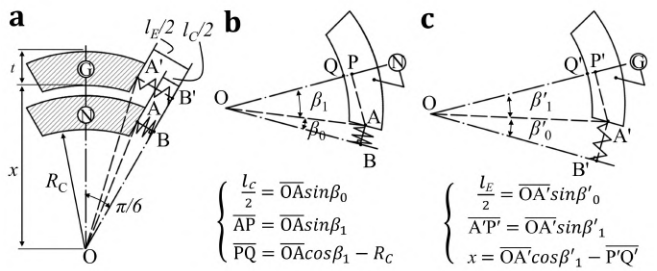

Fig. 3. Design conditions for the connections between new and grown TMs. (a) the outer ring (G), cell of grown TMs; the inner ring (N), cell of new TMs; x, inner radius of grown TMs; t, thickness of cells; R_c, radius of the cells; l_E, length of elongated radial SRBs; l_C, length of compacted radial SRBs; $\pi/6$, radial angle between cells axes and SRBs. (b) The mathematical relationships for the cells of new TMs: β_1, radial angle between $\overline{OP}$ and $\overline{OA}$; β_0, radial angle between $\overline{OA}$ and $\overline{OB}$. (c) The mathematical relationships for the cells of grown TMs: β'_1, radial angle between $\overline{OP}'$ and $\overline{OA}'$; β'_0, radial angle between $\overline{OA}'$ and $\overline{OB}'$.

X) serves the connection between new TMs, and the other side (Fig. 2c XI) between growing and grown TMs.

Initially, new TMs are all compressed and sequentially connected for module delivery. After the axial tip displacement and radial enlargement, the growing TMs connect to the grown TMs and build the physical body. New TMs are delivered through the inner passage of grown TMs. To achieve this, the outer diameter of new TMs must be smaller than the inner diameter of grown TMs (Fig. 3a). That means the sum of radius (R_C) and thickness (t) of the cells should be smaller than the inner radius of grown TMs (x) following the design formula $R_C + t \leq x$.

There are some mathematical relationships between the cells of new (Fig. 3b) and grown (Fig. 3c) TMs. Specifically, the quadrangle composed of the SRBs cells axes with the vertical lines from their conjunction can be split into two triangles originating from the center (O) to the conjunction (A or A′). The relevant triangles then lead to the following additional relations for the cells of new and grown TMs: $\overline{AP} = \overline{A'P'}$, $\overline{PQ} = \overline{P'Q'}$, $\pi/6 = \beta_1 + \beta_0 = \beta'_1 + \beta'_0$, where the radial angle between the axes of cells and SRBs was $\pi/6$. Combining the relations above, it follows that cell thickness (t) must be smaller than the stroke length of radial SRBs (i.e., the length difference between elongated (l_E) and compacted (l_C) SRBs), $t \leq l_E - l_C$.

C. Hydraulic Actuation System

The hydraulic actuation system consists of two expansion actuators, designed for radial expansion, and one elongation actuator (Fig. 4). The expansion actuator (EA) includes six reversible linear actuators, each of which has an expansion head, a spring, a spindle flange, a rubber piston, and a cylinder. The expansion heads are pushed out when the actuator chamber is pressurized, and contract back (with the help of spring force) after the hydraulic pressure is removed. The elongation actuator uses three parallel linear cylinders connected to the EA I. The linear cylinders actuate the ball joint linkages when

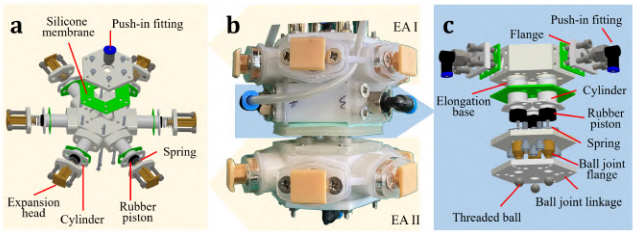

Fig. 4. Hydraulic actuation system. (a) Design of the radial expansion actuator (EA). (b) The assembled prototype. (c) Design of the axial elongation actuator.

the channels inside the elongation base are pressurized. Thanks to the ball joint mechanism, the three parallel linear cylinders can make the ball joint flange and the EA II bend at different angles, resulting in the actuation of TM axial elongation at specific bending angles. Likewise, the hydraulic pressure and the spring force produce the reversible movement of linear cylinders. The hydraulic actuation system fits the size of TMs.

D. Prototype Fabrication

SRBs were fabricated via an FDM 3D printer (Prusa i3 MK3S+, Prusa Research) with a 0.25 mm nozzle. Polypropylene was selected among different thermoplastic and thermoset materials due to its balanced toughness and flexibility. The cells were fabricated by an SLA printer (Formlab 2, Formlabs Inc.) using the Model resin, and their surfaces were polished to improve smoothness. Then, cells and SRBs were glued together to form the TMs.

The structural components of the hydraulic actuation system were fabricated by the same SLA printer with Rigid resin. Other components like flanges and linkages were CNC machined using Teflon. Silicone membranes were fabricated by molding using silicone rubbers (Dragon Skin 30, Smooth-On). The assembled hydraulic actuation system was sealed with molded silicone membranes and tested without any leakage up to 0.8 MPa.

E. Characterization and Demonstration of Prototypes

To characterize the elongation properties, SRB samples were 3D-printed, adding grip sections at both ends to be clamped and then stretched by the Universal Testing Machine (Zwick/Roell Z005, Zwick Roell Group) using a 1 kN load cell. The elongation energy (U_E) was calculated using the area (A_c) underneath the force-elongation curve [26]:

$$A_c = \sum_{i=1}^{n-1} \left(\frac{F_i + F_{i+1}}{2} \right) (D_{i+1} - D_i) \quad (1)$$

where F_i is the force at the ith point, F_{i+1} is the force at the $i+1$th point, D_i is the Universal Testing Machine clamp displacement at the ith point, D_{i+1} is the corresponding value at the $i+1$th point, n is the number of data points.

SRBs were tested with one, two, three, and four convolutions to evaluate the influence of the convolution number on the elongation properties. In this test, the

other parameters were fixed to T_1 = 0.25 mm, T_2 = 0.5 mm, D_0 = 6 mm, and β = 80°. Then, considering the machinability and size constraint for the SRB design, we produced different SRB samples with a single convolution and varied the other parameters. All tested combinations are shown in Table I. Each elongation test lasted until the sample was fully stretched. Five repetitions were performed for each test, and the tensile speed was set at 6 mm/min.

TABLE I

CONVOLUTION PARAMETERS TESTED.

T_1 [mm]	T_2 [mm]	D_0 [mm]	β [°]
0.20, 0.25, 0.30, 0.35	0.5	6	80
0.25	0.3, 0.4, 0.5, 0.6	6	80
0.25	0.5	6, 7, 8, 9	80
0.25	0.5	6	60, 70, 80, 90

Radial expansion, axial elongation, and load-bearing tests were conducted to characterize the SRBs-based TMs. A setup was developed for radial expansion, including a single expansion actuator connected with a hydraulic supply unit. Water was used as medium, and hydraulic pressure was generated by a syringe pump realized with a 12 ml syringe pushed by the Universal Testing Machine. The pressure was recorded by a pressure sensor (ABPLLNT010BGAA5, Honeywell) connected to a data acquisition board (NI-USB-6218, National Instruments). A half TM was used for the radial expansion tests at a 0.2 ml/s flow rate. The expansion pressure and energy (the area underneath the pressure-volume curve) were obtained to characterize the radial expansion of TMs. Analogously, a setup was developed to characterize the axial elongation of TMs. The setup was directly connected to the load cell on the Universal Testing Machine, which provided the elongation power. The TMs were axially elongated at a 6 mm/min elongation rate in radially expanded conditions. The elongation force and displacement were recorded and mapped into the equivalent hydraulic pressure and energy (used to characterize the axial elongation of TMs) as from [27]. To characterize the TMs robustness, one-dimensional compression was used for the load-bearing test. The full TMs were compressed at 6 mm/min by a 120 mm diameter plate on the tensile machine in expanded and elongated conditions. The load-bearing force and displacement were recorded to characterize the prototyped TM-A and TM-B:

$$P_E = F_e / A_E \tag{2}$$

$$Q_E = v_e \times A_E \tag{3}$$

where P_E is the equivalent elongation pressure, F_e is the elongation force, A_E is the equivalent section areas of the linear cylinders, Q_E is the equivalent flow rate, v_e is the elongation rate.

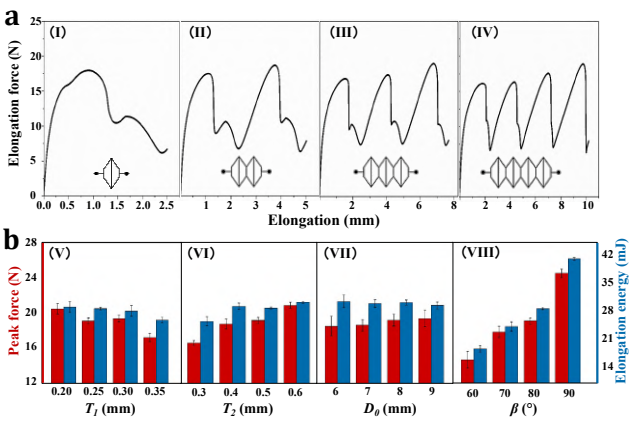

Fig. 5. Results of tensile tests for SRBs. (a) Typical force-elongation curves for SRBs with: (I) one, (II) two, (III) three and (IV) four convolutions. (b) Peak force and elongation energy of SRBs, as influenced by the convolution parameters: (V) thin wall thickness (T_1); (VI) thick wall thickness (T_2); (VII) diameter (D_0); (VIII) convolution angle (β).

Finally, a preliminary demonstration was conducted to show growth, expansion, and elongation potentiality of the TMs. Specifically, an expanded and elongated TM was fixed on a plate as the grown TM, a new TM displaces at the tip, radial expand, and axial elongation with different bending angles and directions.

III. RESULTS AND DISCUSSION

A. Experimental Characterization for SRBs

At the current developmental stage, we aimed to identify a suitable SRB configuration in the design space of the described parameters. Typical force-elongation curves for SRBs with one, two, three, and four convolutions are presented in Fig. 5a. With a single convolution (Fig. 5a(I)), the elongation force first increases and then decreases while increasing elongation. A peak appears when the convolution switches from compacted to an elongated stable state, consistently with the bistability property of the proposed bellow structures, which differs from the increasing trend between force and elongation usually provided by traditional bellows [28], [29]. The curves for SRBs with two, three, and four convolutions contained two, three, and four peaks, respectively (Fig. 5a(II), Fig. 5a(III), and Fig. 5a(IV)). The peaks occurred in a random sequence when each convolution switched stable states. A synchronous switch unlikely can occur due to small variations in convolution fabrication. Peak values are similar apart from a slight increase over the sequential switch. This is likely because the convolution structure at the compacted state is more flexible than the elongated state. The obtained results demonstrate that the bistability evolves into multistability when SRBs have more convolutions and that the convolution number has little influence on the elongation properties of SRBs. Fig. 5b shows SRBs peak force and elongation energy with a single convolution but different convolution parameters. The rise of T_2 (Fig. 5b(VI)) and β (Fig. 5b(VIII)) causes

TABLE II

PROTOTYPED SRBS, TMS, AND HYDRAULIC ACTUATOR.

	Features	Values
SRBs	Thin wall thickness T_1	0.3 mm
	Thick wall thickness T_2	0.5 mm
	Diameter D_0	6 mm
	Convolution angle β	80°
	Number of convolutions	4
	Range of the length for radial SRBs	11-21 mm
	Range of the length for axial SRBs	18-28 mm
TMs	Number of cells (positive and negative cell I and II)	12
	Number of radial SRBs	12
	Number of axial SRBs	3
	Radius of cells R_C	45 mm
	Thickness of cells t	10 mm
	Range of the length	42-52 mm
	Range of the bending angle	0-8.1°
Actuation system	Dimension	Φ70×60 mm
	Hydraulic medium	Water
	Maximum working pressure	0.8 MPa
	Number of reversible linear actuators	12
	Stroke of the reversible linear actuator	0-14 mm
	Number of parallel linear cylinders	3
	Stroke of the parallel linear cylinder	0-8 mm
	Range of the bending angle	0-16.5°

an increment of both peak force and elongation energy. Particularly, with a convolution angle greater than 80°, the peak force and elongation energy notably increment with rates of 28.1% and 43.0%, respectively. An increment of D_0 (Fig. 5b(VII)) also increases the peak force, but the elongation energy remains stable. Finally, rising T_1 (Fig. 5b(V)) decreases the peak force and elongation energy. Results demonstrate that peak force and elongation energy have higher correlations with the convolution angle than thin and thick wall thickness and diameter.

B. Prototypes of Transformable Modules and Hydraulic Actuation System

Based on the SRB characterization, we fixed the design parameters to prototype two mock-up modules considering the convolution angle ($\beta = 80°$) as a compromise between energy cost and force achieved, the wall thicknesses ($T_1 = 0.3mm$ and $T_2 = 0.5mm$) to keep mechanical stability, the diameter ($D_0 = 6mm$) to engage a minimal amount of material, and the number of convolutions (equal to 4) to exploit the maximal elongation stroke. Features of the prototyped SRBs, TMs, and hydraulic actuation system are illustrated in Table II. Overall, the dimensions of the TMs and the hydraulic actuation system match, and the actuation range of the hydraulic actuation system completely covers the transformation range of TMs. The maximum bending angles are 8.1° and 16.5° for the TMs and the hydraulic actuation system, respectively, if one linear cylinder is fully extended and the other two are retracted.

C. Experimental Characterization of Radial Expansion, Axial Elongation, and Load-Bearing

The TM radial expansion characterization (Fig. 6a) shows a zigzag curve with 24 pressure peaks obtained when the half TM is completely expanded. The 24 convolutions from the six radial SRBs radially elongated in a random sequence, each producing a peak on the curve and fluctuating energy consumption. The peak pressure has an averaged inflation at about half of the expansion, probably due to a slightly different bellows stiffness. The final maximum hydraulic pressure was 0.19 MPa. The TM axial elongation characterization shows (Fig. 6b) four major peaks, each followed by two minor peaks in the curve of equivalent elongation pressure. A single TM has three axial SRBs, each containing four convolutions. As a result, the convolutions sequentially elongated, producing the four distinct major peaks, and the three SRBs elongated one after the other, producing the minor peaks with a time interval smaller than between major peaks. The four major peaks have almost the same value, and the maximum equivalent hydraulic pressure was 0.12 MPa using the prototyped elongation actuator. Although the minor peaks of elongation pressure in the triple parallel convolutions had some differences, similar values of elongation energy were still obtained (Fig. 6b).

Fig. 6c shows the results of load-bearing tests for one TM-A and one TM-B. There are four major peaks for both curves when TMs are fully compressed. Overall, the curves exhibit similar behaviors, although a slight variation in values is observed for the second and third peaks, possibly due to manufacturing variations. The maximum load-bearing force, representing the ability of TMs faced with external resistance, was nearly 24 N at the first peak.

D. Growth Demonstration of Prototypes

Results demonstrated that the simplified mechanism possessed the key capabilities we aim to address with the proposed growing robot concept: one-cycle growth of axial tip motion, TM radial expansion, axial elongation, and bending (Fig. 6d-e and Movie S1). Starting from the initial conditions (Fig. 6d(I)), the linear hydraulic cylinder pushed by a tensile machine helped the hydraulic actuation system to axially move and internally slide across the grown TMs, reaching the tip with a new TM (Fig. 6d(II)). Then, the new TM was radially expanded and successfully connected with the grown TM (Fig. 6d(III)) using the expansion actuators. At the end of one cycle, the expanded TM was axially elongated by the elongation actuator (Fig. 6d(IV)) in straight (Fig. 6e(V)) and bent configurations (Fig. 6e(VI-VIII)). The TM can bend on six different angular planes (rotated by 60° from one another) by pressurizing the three axial hydraulic pressure chambers (two high and one low or two low and one high pressure) and consequently differentially elongating the axial SRBs opposite to the corresponding angular directions. For simplicity, the cases reachable with one high pressure chamber control are represented in Fig. 6e. Because of gaps between expansion actuators and TMs left for assembly, the elongation difference between elongated and compacted SRBs was only 5 mm (the length of two convolutions) with a corresponding bending of ~4° with one module, less than the theoretically achievable value (8.1°). Reaching the expected bending is prevented by the

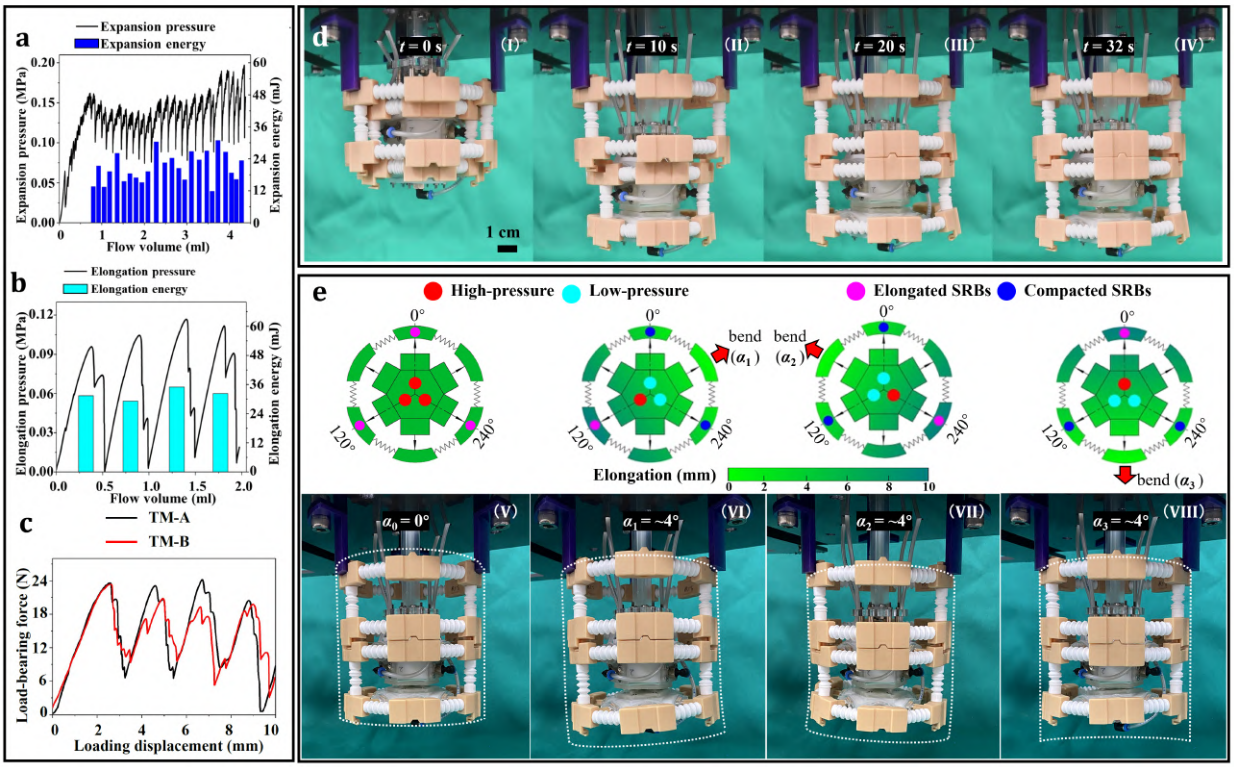

Fig. 6. Characterization of (a) radial expansion, (b) axial elongation, and (c) load-bearing for TMs. (d-e) Growth demonstration. Two pressure levels are adopted: high and low. Straight elongation is reached with all three axial cylinders at high pressure. A bending is reached by injecting high pressure only in one (or two) hydraulic chambers. (d) One-cycle growth with axial elongation. (I) The initial condition; (II) axial tip motion; (III) TM radial expansion; (IV) TM axial elongation. (e) Four different final configurations reached with the modules (downward side) and the corresponding actuation (upward side). (V) The tip module grew straight ($\alpha_0 = 0°$); (VI) the tip module grew with a bending angle ($\alpha_1 = \sim 4°$) on the 120° angular plane; (VII) the tip module bent ($\alpha_2 = \sim 4°$) on the 240° angular plane; (VIII) the tip module bent ($\alpha_3 = \sim 4°$) on the 0° angular plane.

presence of the TM enclosed in the bending module and the internal rigid hydraulic actuator. Increasing the gap between open TM and internal components would relax this limit.

IV. Conclusions

We propose a novel concept of growing robots inspired by plant modular and transformability. This paper focused on developing and characterizing a preliminary implementation, demonstrating one-cycle growth with a two-module assembly. We showcase the axial lengthening of the structure through the apical addition of one module, the module radial expansion, axial elongation, and bending. The prototyped mock-up encloses Transformable Modules (TMs) embedding a newly developed component named Shape-Retention Bellows (SRBs). SRBs are multistable structures that imprint axial and radial transformation and retain the shape after force removal, differently from traditional bellows that recover their shape when external forces are removed. Furthermore, the simultaneous capability to expand and elongate distinguishes TMs from previous transformable structures that can only be expanded in one direction. Because of their unique properties, SRBs and TMs can potentially empower soft robots with, e.g., adaptive actuators and grippers. A modular transformability can benefit future growing robots by providing greater reconfigurability in a post-growth stage by reshaping the grown TMs and enhancing morphological adaptation. Yet, the presented prototype necessitates improvements to match the envisioned robot concept. First, the apical motion must be directed by an embedded actuation at the tip; the gap between internal and grown TMs must be increased to permit deformability of grown TMs, improve bending performance and facilitate the passage of modules into bent segments; a more agile manufacturing process must be considered for easiness of production, miniaturization, and robustness; distributed and differentially controllable actuation must be integrated into future solutions. Smart TMs embedded with distributed actuators and sensorized SRBs made of functional materials with advanced manufacturing techniques have the potential to realize precision actuation. Nonetheless, our study gives preliminary cues for the new concept of modular growing robots. We provided important design guidelines to design and distribute multistable structures and deploy modular elements capable of multi-axial transformation. Thanks to the lessons learned through this study, our concept can be further developed, and it could pave the way for a new generation of robots to grow based on modular and reconfigurable principles.

REFERENCES

[1] F. Iida and A. J. Ijspeert, "Biologically inspired robotics," *Springer Handbook of Robotics*, pp. 2015–2034, 2016.

[2] A. Sadeghi, A. Mondini, E. Del Dottore, V. Mattoli, L. Beccai, S. Taccola, C. Lucarotti, M. Totaro, and B. Mazzolai, "A plant-inspired robot with soft differential bending capabilities," *Bioinspir. Biomim.*, vol. 12, no. 1, p. 015001, 2016.

[3] I. Must, E. Sinibaldi, and B. Mazzolai, "A variable-stiffness tendril-like soft robot based on reversible osmotic actuation," *Nat. Commun.*, vol. 10, no. 1, p. 344, 2019.

[4] B. Su, S. Gong, Z. Ma, L. W. Yap, and W. Cheng, "Mimosa-inspired design of a flexible pressure sensor with touch sensitivity," *Small*, vol. 11, no. 16, pp. 1886–1891, 2015.

[5] G. Y. Bae, S. W. Pak, D. Kim, G. Lee, D. H. Kim, Y. Chung, and K. Cho, "Linearly and highly pressure-sensitive electronic skin based on a bioinspired hierarchical structural array," *Adv. Mater.*, vol. 28, no. 26, pp. 5300–5306, 2016.

[6] E. Sinibaldi, A. Argiolas, G. L. Puleo, and B. Mazzolai, "Another lesson from plants: the forward osmosis-based actuator," *PloS One*, vol. 9, no. 7, p. e102461, 2014.

[7] E. Sinibaldi, G. Puleo, F. Mattioli, V. Mattoli, F. Di Michele, L. Beccai, F. Tramacere, S. Mancuso, and B. Mazzolai, "Osmotic actuation modelling for innovative biorobotic solutions inspired by the plant kingdom," *Bioinspir. Biomim.*, vol. 8, no. 2, p. 025002, 2013.

[8] F. Meder, S. P. M. Babu, and B. Mazzolai, "A plant tendril-like soft robot that grasps and anchors by exploiting its material arrangement," *IEEE Robot. Autom. Lett.*, vol. 7, no. 2, pp. 5191–5197, 2022.

[9] W. Wang, C. Li, M. Cho, and S. H. Ahn, "Soft tendril-inspired grippers: shape morphing of programmable polymer–paper bilayer composites," *ACS Appl. Mater. Interfaces*, vol. 10, no. 12, pp. 10 419–10 427, 2018.

[10] I. Fiorello, O. Tricinci, G. A. Naselli, A. Mondini, C. Filippeschi, F. Tramacere, A. K. Mishra, and B. Mazzolai, "Climbing plant-inspired micropatterned devices for reversible attachment," *Adv. Funct. Mater.*, vol. 30, no. 38, p. 2003380, 2020.

[11] D. Lunni, M. Cianchetti, C. Filippeschi, E. Sinibaldi, and B. Mazzolai, "Plant-inspired soft bistable structures based on hygroscopic electrospun nanofibers," *Adv. Mater. Interfaces*, vol. 7, no. 4, p. 1901310, 2020.

[12] B. Mazzolai, L. Beccai, and V. Mattoli, "Plants as model in biomimetics and biorobotics: new perspectives," *Front. Bioeng. Biotechnol.*, vol. 2, pp. 1–5, 2014.

[13] E. Del Dottore, A. Sadeghi, A. Mondini, V. Mattoli, and B. Mazzolai, "Toward growing robots: a historical evolution from cellular to plant-inspired robotics," *Front. Robot. AI*, vol. 5, p. 16, 2018.

[14] B. Mazzolai, A. Mondini, E. Del Dottore, and A. Sadeghi, "Self-growing adaptable soft robots," *Mechanically Responsive Materials for Soft Robotics*, pp. 363–394, 2020.

[15] A. Sadeghi, A. Tonazzini, L. Popova, and B. Mazzolai, "A novel growing device inspired by plant root soil penetration behaviors," *PloS One*, vol. 9, no. 2, p. e90139, 2014.

[16] A. Sadeghi, A. Mondini, and B. Mazzolai, "Toward self-growing soft robots inspired by plant roots and based on additive manufacturing technologies," *Soft Robot.*, vol. 4, no. 3, pp. 211–223, 2017.

[17] A. Sadeghi, E. Del Dottore, A. Mondini, and B. Mazzolai, "Passive morphological adaptation for obstacle avoidance in a self-growing robot produced by additive manufacturing," *Soft Robot.*, vol. 7, no. 1, pp. 85–94, 2020.

[18] M. M. Hausladen, B. Zhao, M. S. Kubala, L. F. Francis, T. M. Kowalewski, and C. J. Ellison, "Synthetic growth by self-lubricated photopolymerization and extrusion inspired by plants and fungi," *Proc. Natl. Acad. Sci.*, vol. 119, no. 33, p. e2201776119, 2022.

[19] E. W. Hawkes, L. H. Blumenschein, J. D. Greer, and A. M. Okamura, "A soft robot that navigates its environment through growth," *Sci. Robot.*, vol. 2, no. 8, p. eaan3028, 2017.

[20] A. Martín-Barrio, J. del Cerro, A. Barrientos, and H. Hauser, "Emerging behaviours from cyclical, incremental and uniform movements of hyper-redundant and growing robots," *Mechanism and Machine Theory*, vol. 158, p. 104198, 2021.

[21] O. E. Jensen and J. A. Fozard, "Multiscale models in the biomechanics of plant growth," *Physiology*, vol. 30, no. 2, pp. 159–166, 2015.

[22] E. Kolb, V. Legué, and M.-B. Bogeat-Triboulot, "Physical root–soil interactions," *Physical biology*, vol. 14, no. 6, p. 065004, 2017.

[23] F. E. Putz and N. M. Holbrook, "Biomechanical studies of vines," *The biology of vines*, pp. 73–97, 1991.

[24] H. Hauser, "Resilient machines through adaptive morphology," *Nature Machine Intelligence*, vol. 1, no. 8, pp. 338–339, 2019.

[25] M. Zhang, J. Liu, Y. Wang, L. An, M. D. Guiver, and N. Li, "Highly stable anion exchange membranes based on quaternized polypropylene," *J Mater. Chem. A*, vol. 3, no. 23, pp. 12 284–12 296, 2015.

[26] D. Rahmatabadi, M. Pahlavani, A. Bayati, R. Hashemi, and J. Marzbanrad, "Evaluation of fracture toughness and rupture energy absorption capacity of as-rolled lz71 and lz91 mg alloy sheet," *Mater. Res. Express*, vol. 6, no. 3, p. 036517, 2018.

[27] K. A. McCulloh and J. S. Sperry, "Patterns in hydraulic architecture and their implications for transport efficiency," *Tree Physiol.*, vol. 25, no. 3, pp. 257–267, 2005.

[28] E. Filipov and M. Redoutey, "Mechanical characteristics of the bistable origami hypar," *Extreme Mech. Lett.*, vol. 25, pp. 16–26, 2018.

[29] L. Wang and Z. Wang, "Mechanoreception for soft robots via intuitive body cues," *Soft Robot.*, vol. 7, no. 2, pp. 198–217, 2020.